Development of Informative Path Planning for Inspection of the Hanford Tank Farm

Sebastián A. Zanlongo[1], Leonardo Bobadilla[1], Dwayne McDaniel[2], Yew Teck Tan[2]

***Abstract*— Traditional environmental and structural monitoring often uses static sensor networks deployed at predetermined locations or mobile robots that use a rastering technique for area coverage. These methods rely on the operators making assumptions about the nature of the unknown field that is being measured and are often time-consuming for localizing an area of interest. Here, we aim to quickly localize possible leaks within high-level nuclear waste tanks at the Hanford facility. The structure of these tanks precludes most sensor network approaches and raises many issues with robotic inspection, such as navigation within highly constrained environments. This work uses a Bayesian Optimization approach for guiding a mobile robot's search strategy and implements a utility function that allows for prior knowledge of the structure to be incorporated when selecting future search locations. Compared to traditional exhaustive approaches, our method quickly reduces RMSE error and shortens the distance the robot must travel.**

I. INTRODUCTION

During World War II and the Manhattan Project, large amounts of high-level radioactive waste were generated. Some of these wastes are in liquid form and stored in large double-shell tanks at the Hanford Facility in Washington state. These structures are now in a surveillance and maintenance phase requiring continuous monitoring to check for containment failures. Contamination of these and similar structures can result from leakage, and one tank has been confirmed to have leaked [1].

Localizing the source of these potential leaks is difficult due to the structure of the tank: the tanks are buried approximately 4.5m underground, and the bottom of the tank is another 14m deeper with a diameter of 23m, as illustrated in Figure 2(a) [2]. Inspection of the structural integrity of the tanks can only be accessed via narrow annuli at ground level, further complicating sensor deployment. Moreover, this only serves to reach the tank along its perimeter. Access to the rest of the tank bottom must be done through a series of narrow $\sim$4cm cooling refractory slots located at the bottom of the tank. We might consider deploying a sensor network throughout the refractory slots. However, the sensors may interfere with the air being circulated through the slots, or the moving air could dislodge the sensors. Moreover, deployment in such a constrained environment faces the issues of how to transport and attach the sensors, and how to power and communicate with them over extended periods. Existing inspection approaches use a pole-mounted camera; however, this can only inspect the perimeter of the tank and the outermost segment of the refractory slots. Furthermore, pole-mounted visual inspection requires that operators manually inspect each of the refractory slots [3], leading to a labor-intensive, time-consuming process.

There are sampling methods such as [4] which attempt to perform a spatial extrapolation given samples at selected discrete locations. Care must be taken when selecting and adapting a sampling approach, as an inappropriate regression model or utility function may cause problems ranging from non-representative samples to overlooking an important location. Furthermore, inaccurate estimations of the spatial variability can lead to incorrect modeling of the underlying field and contamination properties.

In this paper, we present a methodology for automating and improving the inspection process of these tanks. We propose an Adaptive Informative Path Planning (IPP) approach that would allow a miniature robotic rover to inspect the tank for locations of interest efficiently. The IPP algorithm incorporates prior knowledge about the tank structure, balances exploration and exploitation to initially locate and then refine the points of interest, and also accounts for the robot's movement constraints.

The rest of the paper is organized as follows: In Section II, we review existing approaches to IPP, including relevant similarities, and the major differences to our domain. In Section III, we define the environment and problem being tackled, and Section IV describes our approach. Sections V and VI cover the simulated trials, and an analysis of the results. In Sections VII and VIII we offer a discussion of the results obtained and final conclusions.

II. RELATED WORK

IPP has broad applicability, used to localize points of interest in forests, oceans, and disaster areas [5], and contains myriad domain-specific issues which can render existing approaches insufficient. Traditional localization such as [6] often uses a rastering (zig-zag) pattern to cover an area to map it, or execute a minimum-cost tour of locations determined to be most informative *a priori* [7]. These approaches may take a long time to localize the source if it is opposite to the starting position.

Adaptive sampling aims to provide better results with less time by actively adapting its sampling locations. In this work, we utilize a modified Gaussian Process - Upper Confidence Bound approach (GP-UCB) [8] to efficiently

[1]Sebastián A. Zanlongo and Leonardo Bobadilla are with the School of Computing and Information Sciences, Florida International University, Miami, FL 33199, USA szanl001@fiu.edu, bobadilla@cs.fiu.edu

[2]Yew Teck Tan and Dwayne McDaniel are with the Applied Research Center, Florida International University, Miami, FL 33199, USA {yetan, mcdaniel}@fiu.edu

select sampling locations. The goal is to deploy a robotic system for localizing radioactive leaks, and thus has some similarities to [9], [10] where robots are fitted with optical and radiation sensors to find radiation sources, and [11] which has a strong showing of aerial vehicles and their associated mapping techniques. The approach in this paper differs in its unique environment and the resulting constraints such as limited robot movement.

Unlike some existing IPP approaches which rely purely on the informativeness of possible sampling locations [12], we also incorporate robot dynamics such as movement and tether constraints that limit the robot's ability to visit specific locations easily. This idea bears some resemblance to work by [13], [14] where a Gaussian Process is used to model both the phenomenon and the quality of possible paths. With regards to path-planning, we look to Brass et al. [15] which performs path planning for a tethered robot given polygonal obstacles, and Kim et al. [16] which use a Multi-Heuristic A^* algorithm to find paths for a tethered robot with a homotopy invariant augmented graph. For the robot to navigate between the vertices in the graph representation of the refractory slots, we use a modified A^* algorithm similar to that of [17].

III. PROBLEM FORMULATION

The goal of inspecting the tanks is to detect anomalies - in this case, leaks. As a proxy for finding the leak, we use the temperature distribution at the bottom of the tank, which would be impacted by the presence of a leak. We seek to create a map of the temperature distribution at the bottom of the tank - which is represented by an unknown scalar field $f : \mathbb{R}^d \to \mathbb{R}$, from samples Y selected from a set of potential sampling locations V. Given the samples, we wish to find the location with the highest temperature, corresponding to the most likely source of a leak. Moreover, we desire to select the sampling locations which best update the model, but also reduce the overall distance traveled while respecting the kinematic constraints of the robot. Complete coverage would map out the entire tank, lending itself to an exhaustive approach. This formulation instead seeks to find the leak more quickly than a traditional exhaustive approach.

The approach and simulation in this work were designed for deployment in the Hanford facility double-shell tanks. These tanks are composed of an inner tank that holds the high-level liquid radioactive waste and an outer shell serving as a fail-safe if the inner tank leaks. Figure 1 illustrates a cutaway view of the tank, indicating the inner storage vessel, refractory slots, and the gap between the inner and outer tank walls. Here, we will describe the structure in further detail.

A. Refractory Slot Structure

Sandwiched between the bottom of the two tanks is a series of air distribution slots seen in Figure 1, also known as refractory slots. This system cools the primary tank and provides an avenue for inspecting the bottom of the inner tank without actually entering the tank itself. The tanks were built over multiple years and have slightly varying refractory slot designs. We focus on the design of the AY-series tanks,

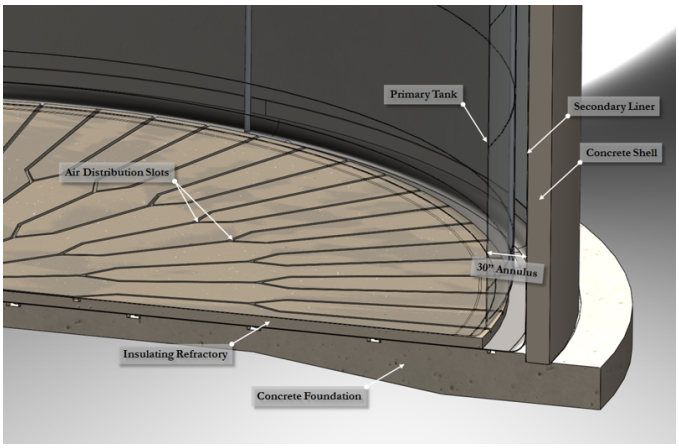

Fig. 1: Tank cutaway showing the inner and outer shells, refractory slots, and annulus at the sides of the tanks.

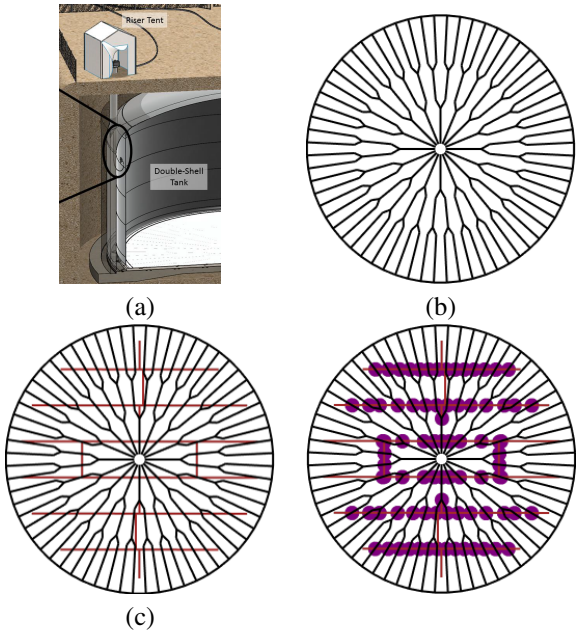

Fig. 2: Tank Structure

(a) Tank cutaway showing buried tank and access annulus. (b) The layout of the refractory slots at the bottom of the tanks. (c) View from (b) with the addition of weld seams. (d) View from (c), with locations where refractory slots intersect weld seams highlighted.

which consist of ∼4cm-wide slots arrayed radially outwards as in Figure 2(b).

We model the refractory slots as a graph, with the slots represented as edges E, and the forks as vertices V. The robot cannot execute tight turns (cannot turn at a fork to go down a parallel slot). Given this graph structure, we only considered vertices as valid sampling locations, rather than the continuous plane representing the tank floor. As such, we introduce additional evenly-spaced vertices along edges such that a minimum desired sampling resolution is achieved.

The bottom of the tank is formed by multiple steel plates welded together, meaning that there are weld seams between

the various plates. These weld seams run in a pattern as in Figure 2(c), with occasional overlaps along the refractory slots indicated by the purple points in Figure 2(d). Many of the seams had initial high rejection rates, and have been reworked [18]. Due to the rework, their integrity may be compromised, making them of higher interest.

B. Temperature Distribution Modeling

Searching for the leak, we might initially consider searching for the liquid that has leaked out. However, there are confounding factors such as seepage from other sources, as well as desiring to avoid the robot coming into contact with the contamination. We might also mount a radiation sensor to the robot; however, a typical radiation sensor would not fit within a refractory slot. Moreover, radiation roughly follows an inverse-square law, making localization difficult. Instead, we look towards *temperature* as a proxy measurement as these sensors are small and sensitive to temperature variations. The Gaussian nature of temperature assists in localizing the leak. The source of the leak corresponds to the peak, and moving further away from the leak leads to a decaying signal. The model was generated using a 2-dimensional multivariate normal distribution with a probability density function such as that in [19], with mean vector M, a randomly-generated positive definite covariance matrix Σ. Further details about the model can be found in Section V.

C. Regression

Gaussian Processes provide a method for modeling unknown fields non-parametrically. Here, we aim to efficiently derive a Gaussian Process regression through a process such as that described in [19]. Given a set of N sampling locations, each location $x_i \in \mathbb{R}^2$ has a noisy measurement $y_i \in \mathbb{R}$ given by $y = f(x)+\epsilon$ where $f(x)$ is the ground-truth and $\epsilon \sim \mathcal{N}(0, \sigma_n^2)$. The predicted mean u^* and covariance σ^* at a specific target location $x^* \in X^*$ is given by:

$\mu(x^*) = K(x^*, X)K_X^{-1}y$

$\sigma(x^*) = K(x^*, x^*) - K(x^*, X)K_X^{-1}(X, x^*)$

where $K(X', X'')$ is the covariance matrix, X are the sampled observation locations, and $K_X = K(X, X) + \sigma_n^2 I$.

For the covariance function, our implementation uses a Matérn kernel. This kernel was chosen as a finitely differentiable kernel can better model physical processes, and does not assume as much smoothness as other kernels - such as the infinitely differentiable Squared Exponential kernel - which can yield unrealistically smooth results when modeling a physical process [20]. The Matérn kernel is described as:

$$k(x_i, x_j) = \sigma^2 \frac{2^{1-\nu}}{\Gamma(\nu)} \left(\sqrt{2\nu} \frac{d}{\rho} \right)^{\nu} K_\nu \left(\sqrt{2\nu} \frac{d}{\rho} \right) \quad (1)$$

Here, x_i, x_j are two locations and d is the distance between them, which is parameterized by $\rho > 0$. We control the smoothness of the function via $\nu > 0$. Γ is the gamma function, and K_ν is the modified Bessel function of the second kind [19]. We select $\nu = 1.5$ (a once-differentiable function) to avoid having to compute the Bessel function, allowing for a roughly 10 times faster computation. For optimizing the kernel's parameters, we use the Limited-memory BFGS (L-BFGS-B) [21] optimization algorithm, which has linear memory usage. The first run of L-BFGS-B is done with the kernel's initial parameters, and then an additional n restarts using θ derived from a random log-uniform distribution within the allowed bounds.

D. Robot

In this work, we model the robot as a point robot, capable of moving along edges in the graph from one vertex to another. To simplify the problem, we assumed a movement speed of 0.3m/s and a sampling time of 10s when measuring the temperature at a location. The robot has a tether, which was selected to be long enough to allow the robot to access any point in the refractory slots, but short enough that the furthest location would require using all the length of the tether with minimal slack. This tether is needed to:

- Power the robot
- Send / receive commands and sensor data
- Allow for removal of robot in event of system failure

The tether limits the distance the robot can travel and constrains its movement (loops and tight turns are not possible). The most noticeable effect of the tether is that the robot cannot completely circle the tank, and must instead retract to the insertion point and then go the other direction when reaching locations on the far side of the tank. This constraint can be seen in Figure 3(d), where the robot must circle back before exploring the other half of the tank.

IV. GAUSSIAN PROCESS MODELING AND SAMPLING LOCATION SELECTION

We begin by accepting as input a graph ($G = (V, E)$) representation of the refractory slots, and discretizing the graph to the desired resolution by inserting additional vertices along the edges as needed. This process allows us to approximate the continuous sampling space using a simpler discrete representation. The vertices also encode the angles between each other, preventing the robot from attempting tight turns which would cause the tether to become stuck.

These restrictive constraints permit the solution to be used in similar environments such as the tanks at the Savannah River National Laboratory [22], or the Waste Isolation Processing Plant (WIPP), which also has a channel-like structure. This method can also be applied to more traditional open environments. If a graph structure is not initially available, a Voronoi decomposition or cell decomposition [23] may be used to generate a graph.

The approach consists of a modified Upper Confidence Bound algorithm: Given the current state of a Gaussian Process Regression, we use the predictive output mean μ^* *(Exploitation)* and variance σ^* *(Exploration)* at the candidate sampling locations $\mathcal{S}$, which is initially equivalent to V. Weld seam bias w serves to increase the expected utility of prospective sampling locations that lie on top of a weld seam, given the expected higher failure rate of weld seams due to their high initial rejection rate.

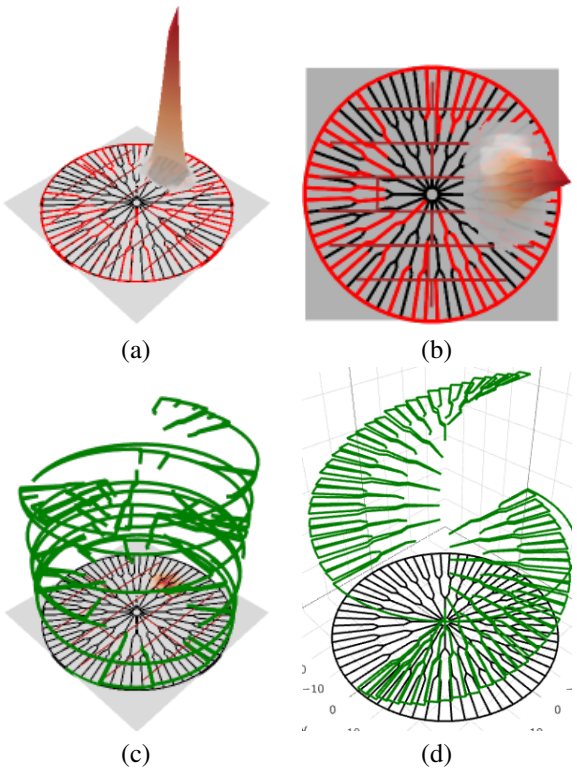

Fig. 3: Example Robot Trajectory

(a) Isometric view of a Gaussian-Process-like temperature distribution (with the peak being the leak source) overlaid on refractory slots. (b) Overhead view of (a). (c) Example time representation of a robot moving through refractory slots, where the vertical z-axis is movement through time. (d) Time representation of a robot moving through refractory slots using an exhaustive approach.

The exploitation and exploration values are normalized at each step $t \in T$, with regards to the highest-valued predicted output in the set S. The weld seam value is set to a constant $w = 1$. These elements are then respectively weighted by λ, where $\forall i \in \lambda | i \in [0, 1]$ to yield: $utility = \lambda \cdot [\mu^*, \sigma^*, w]$, such that $utility \in [0, 3]$, where locations with a higher value are deemed more desirable.

We will now cover each of the parameters in detail, and how they affect the model's behavior.

1) Exploration vs Exploitation: We begin by discussing the most critical component of the modified UCB algorithm: the trade-off between exploration and exploitation.

We start by constructing a distribution that describes the Gaussian Process we are looking to reconstruct. Adding more observations, the distribution improves, and the uncertainty (variance) diminishes near sampled locations allowing us to determine which locations need to be further explored. The UCB algorithm shown in Algorithm 1 is drawn from [13], [24], and selects a new sampling location based on the weighted mean and variance. A higher mean biases to rapid localization and a higher variance to total coverage. This process is done by finding the maximum of the UCB utility function, which serves as a computationally simpler proxy for the task of regression [25], [26]. We must also set α,

Algorithm 1: Bayesian Optimization

Input: Possible sampling locations V, Utility function U, Update Rate r, Number of samples to take n
$S' \leftarrow V$
for $t \in [1, n]$ **do**
    Evaluate $U(s)$ over S'
    $x \leftarrow argmax\ U(s)$
    $Sample(x)$
    $S' \leftarrow S' \backslash x$
    if $t\%r == 0$ **then**
        $UpdateGP(x)$

which is the value added to the diagonal of the kernel matrix when fitting the model. Small values correspond to less noise, whereas high values indicate greater noise, equivalent to using an additional White Kernel. Here, we set $\alpha = 0.2$, which roughly correlates to the $+/-2°C$ error margin of the temperature sensor model.

2) Weld-Seam Bias: The previous section assumes that the only way to gather information is via new samples. However, we know that the weld seams are more prone to failure than the steel plates themselves. With this in mind, we can bias our search to prioritize weld seams that intersect our available sampling locations (Figure 2(d)) by adding the weighted parameter w to the utility function. For vertices that lie on a weld seam $x \in V_{weld}$, we add the weighted w to the utility; otherwise, the value is 0.

V. SIMULATION

Simulation consisted of a series of 200 independent trials, each with a randomly generated hot-spot representing a leak. The hot-spots exhibit a distribution that can be described by a Gaussian Process, and the peak of each hot-spot lies within the bounds of the tank. One hundred of these trials had the hot-spot centered on a randomly-selected location along a weld seam, to reflect the higher failure rate expected of weld seams compared to the plates themselves. The other 100 trials had the hot-spot generated at a random location within the bounds of the tank. A visualization of this can be found in Figure 4.

Without loss of generality, the hot-spot peak intensity (mean) was set to 100, while the covariance along the x, y axes was randomly selected from the range $[4.5, 18]$. This range was selected as $4.5m$ is approximately the maximum distance between two refractory slots - therefore the minimum size for at least one refractory slot to intersects the hot-spot. The upper value of $18m$ corresponds to 4 times 4.5 and was used to provide a varying range of spread. The resulting hot-spot was then used to evaluate the various weighting schemes.

While executing a trajectory, the robot would sample if it visited a previously un-sampled location, and remove that location from the candidate pool of future sampling locations S. The regression was fitted at every 3^{rd} new sample. This process continued until all vertices in the graph had been

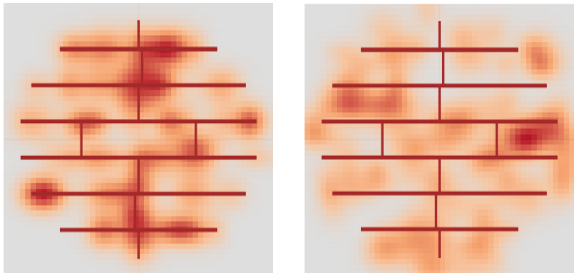

(a) (b)

Fig. 4: Example visualization of distributions.

(a) Averaged location of distributions centered on a random location coinciding with a weld-seam over 100 trials. (b) Averaged location of distributions placed randomly throughout the tank over 100 trials. On average 3ft away from the nearest weld seam.

visited and sampled. Apart from IPP, an exhaustive approach was executed against the same distributions to establish a baseline. The exhaustive approach used the trajectory shown in Figure 3(d) where x, y are the planar coordinates, and z represents time.

The algorithm terminates when there are no more sampling locations. An operator could ostensibly specify stopping criteria of either a minimum overall variance or if a high enough signal is found (which would be known ahead of time given the contents of the tank).

VI. ANALYSIS

Testing of the different weighting schemes was done by comparing their Root Mean Square Error (RMSE) for the predicted value at locations throughout the tank, defined as: $RMSE(\mu) = \sqrt{\frac{1}{n}\sum_{i=1}^{n}(Y_i - \hat{Y}_i)^2}$ where Y is the vector of ground-truth values, and $\hat{Y}$ is the vector of n predictions.

The resulting non-negative loss-value is a measure of accuracy indicating the difference between the predicted values and the ground truth, where a value of 0 is the best score, and larger values correspond to a worse-performing model. We will also refer to "local RMSE" as the RMSE for a region surrounding the distributions' center, with a diameter of 1σ, the spread given by the covariance of the distribution. This is done to illustrate the performance of the regression for the point of interest, rather than the entire area.

A. Illustrative Examples

In this section, we outline the weighting schemes that best illustrate how different strategies can affect the performance of the approach described above.

1) Randomly-Located Leaks: We begin by focusing on a model tank where the leak is generated at a random location. In Figure 5, we compare the average performance among the different weighting schemes across the 100 trials. The y-axis indicates the average local RMSE score every time the regression was updated, and the x-axis shows the average time-step at which the regression was updated across all trials. The models initially begin at an RMSE of approximately 31.

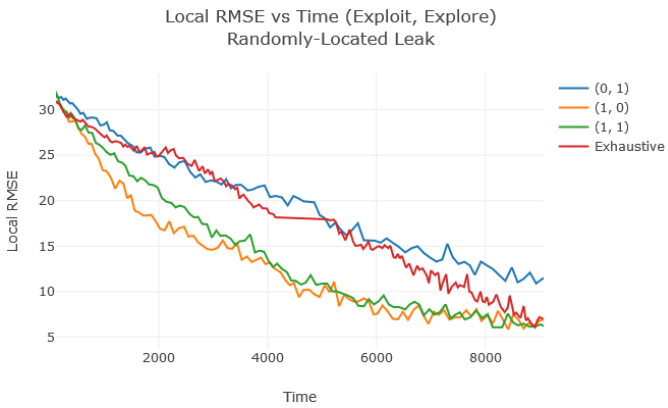

Fig. 5: RMSE performance of various weighting schemes given leaks created in random locations throughout the tank. The y-axis corresponds to the RMSE, and the x-axis indicates the average sampling step at which the corresponding score was achieved.

As the leaks are randomly-located, the weld-seam weight is set to 0 in all cases. The traditional exhaustive approach performs as expected, with a steady decrease in the local RMSE. An Exploration-based approach of $\lambda = [0, 1, 0]$ will naturally perform poorly, as this will make the robot alternate between each side of the tank to visit the largest remaining unexplored region. Switching over to an Exploitation-based approach of $\lambda = [1, 0, 0]$, we find a remarkably better performance than either the exploration or exhaustive methods as the robot quickly converges on the location with the highest temperature. Attempting to combine exploration and exploitation as $\lambda = [1, 1, 0]$ results in the robot occasionally moving to distant parts of the tank which have high uncertainties.

2) Weld-Seam-Biased Leaks: We now turn our attention to the trials where the leaks were created over weld-seams. The accompanying results can be found in Figures 6, 7. The baseline using the exhaustive approach closely resembles that of the previous trials with a randomly-located distribution, beginning at an RMSE of $\sim$31, and eventually decreasing to $\sim$5. However, we are primarily concerned with how quickly we can localize the leak. If we consider the threshold to be a 50% reduction in the local RMSE (to be conservative, an RMSE of 15), then an exhaustive approach reaches this threshold at sampling step $6,147$. Using the previous-best weighting scheme of $[1, 0, 0]$, we reach a $> 50\%$ reduction of the local RMSE by step $3,257$, or almost half the time of the exhaustive method. Taking into account our prior knowledge about weld-seams having a higher failure rate, we compare this with $\lambda = [1, 0, 1]$. Incorporating prior knowledge provides a slight advantage, shaving off 21% of the exploitation approach to a sampling step of $2,584$, or almost 42% of the exhaustive approach. Incorporating the exploration weight ($\lambda = [1, 1, 1]$) again shows the same issue as before, giving slightly worse results.

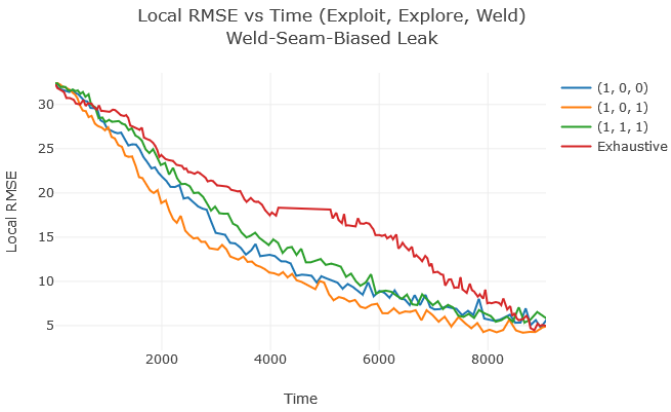

Fig. 6: RMSE performance of various weighting schemes given leaks biased to weld-seams. The y-axis corresponds to the RMSE, and the x-axis indicates the average sampling step at which the corresponding score was achieved.

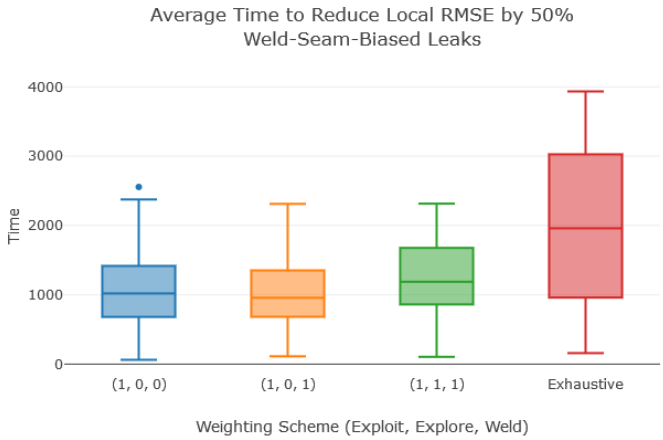

Fig. 7: Sampling steps to reduce the local RMSE to 50% of the original value. Results shown are with regards to weld-seam biased leak locations.

VII. DISCUSSION

A. Path-Planning Considerations

A common theme throughout the results shown above is the harsh implicit penalty for moving. In a continuous plane, a robot can easily move from one location to the next. In the case of the refractory slot structure, moving between locations requires the robot to exit the refractory slot, circle the tank, and then enter a different slot, leading to substantial movement costs. Movement is further constrained by the tether forbidding any turns within the forked refractory slots. Therefore exploration is heavily penalized, as seen in strategies favoring σ.

Readers may notice that the exhaustive approaches have a slight plateau in the middle of their runs. This result is due to the structure of the exhaustive approach path, which must explore one half of the tank, and then circle back before exploring the other half due to the robot's tether constraint. During the circling back of the robot, the regression will be unaffected as those locations have already been sampled.

B. Leak Behavior and Effects on Weighting Performance

The trials shown here were all simulated with a single distribution (representing a single leak). In the event of two or more simultaneous leaks, we expect that slightly favoring Exploration (σ) might yield better performance as it would help in avoiding the robot becoming stuck on a local maximum. In the case of no leaks and even signal distribution, an exploitation approach will tend towards a random walk, and an exploration approach will travel between locations of high variance.

We might also consider situations where the leak takes on an elongated shape. This has not been explicitly modeled; however, we expect that if there is some bias for exploitation, it would seek the peak, and might miss parts of the leak that have a lower intensity. In the future, we plan to examine how the model performs given multiple unknown distributions, including elongated leaks.

C. Performance

As was previously shown in Section VI, we find better performance using an appropriate weighting scheme such as $\lambda = [1, 0, 1]$ than an exhaustive approach. Of interest is not just the overall reduction in the average time needed to localize the point of interest, but also the dispersion. In Figure 7 we show the whisker plot for various schemes when operating in a weld-seam-biased tank. Of particular importance is the high variability of the exhaustive approach, and the lower variability of the UCB techniques.

VIII. CONCLUSIONS

In this paper, we illustrated a methodology for localizing potential leaks at the Hanford Facility high-level waste tank farm. We provide simulation results and an analysis of the results indicating that the solution is feasible and reduces time compared to a traditional rastering exhaustive approach. The solution works with a tether constraint and utilizes a weighting matrix to allow for operator-defined bias towards exploration or exploitation easily. This work can also be used when surveying other types of structures and buildings, allowing for effective remote characterization, assisting operators to make better decisions about what areas need decontamination. We have also developed the robotic mini-rover with a video camera and performed preliminary testing in mock-up refractory slots [27], [28]. We are now working to integrate temperature and other sensors. Future directions for this work include deployment within the actual working tanks, and applying these techniques to a radiation signal rather than temperature.

ACKNOWLEDGMENTS

This material is based upon work supported by the Department of Energy Office of Environmental Management under the DOE-FIU Cooperative Agreement DE-EM0000598. This material is also based in part upon work supported by the U.S. Department of Homeland Security under Grant Award Number 2017-ST-062-000002.

REFERENCES

[1] J. K. Engeman, C. L. Girardot, D. J. Harlow, and C. L. Rossenkrance, *Tank 241-AY-102 Leak Assessment Report*. 2012.

[2] J. Gunter, "Hanford review of double-shell tank construction," *ASNT Annual Conference*, Oct 2015.

[3] C. Girardot, "Hanford double-sheel tank visual inspections," *ASNT Annual Conference*, Oct 2015.

[4] G. Hitz, A. Gotovos, M.-É. Garneau, C. Pradalier, A. Krause, R. Y. Siegwart, *et al.*, "Fully autonomous focused exploration for robotic environmental monitoring," in *Robotics and Automation (ICRA), 2014 IEEE International Conference on*, pp. 2658–2664, IEEE, 2014.

[5] N. Cao, K. H. Low, and J. M. Dolan, "Multi-robot informative path planning for active sensing of environmental phenomena: A tale of two algorithms," in *Proceedings of the 2013 international conference on Autonomous agents and multi-agent systems*, pp. 7–14, International Foundation for Autonomous Agents and Multiagent Systems, 2013.

[6] E. W. Michael E. Hosmar, Scott B. Nokleby, "Experimental Testing of an Autonomous Radiation Mapping Robot," *CCToMM Mechanisms, Machines, and Mechatronics (M3) Symposium*, 2017.

[7] G. Hollinger and G. Sukhatme, "Sampling-based motion planning for robotic information gathering," *Robotics: Science and Systems IX*, 2013.

[8] N. Srinivas, A. Krause, S. Kakade, and M. Seeger, "Gaussian process optimization in the bandit setting: No regret and experimental design," in *Proceedings of the 27th International Conference on International Conference on Machine Learning*, ICML'10, (USA), pp. 1015–1022, Omnipress, 2010.

[9] C. Cai, B. Carter, M. Srivastava, J. Tsung, J. Vahedi-Faridi, and C. Wiley, "Designing a radiation sensing uav system," in *Systems and Information Engineering Design Symposium (SIEDS), 2016 IEEE*, pp. 165–169, IEEE, 2016.

[10] K. Qian, A. Song, J. Bao, and H. Zhang, "Small teleoperated robot for nuclear radiation and chemical leak detection," *International Journal of Advanced Robotic Systems*, vol. 9, no. 3, p. 70, 2012.

[11] D. Connor, P. Martin, and T. Scott, "Airborne radiation mapping: overview and application of current and future aerial systems," *International Journal of Remote Sensing*, vol. 37, no. 24, pp. 5953–5987, 2016.

[12] D. Golovin and A. Krause, "Adaptive submodularity: Theory and applications in active learning and stochastic optimization," *Journal of Artificial Intelligence Research*, vol. 42, pp. 427–486, 2011.

[13] R. Marchant and F. Ramos, "Bayesian optimisation for intelligent environmental monitoring," in *Intelligent Robots and Systems (IROS), 2012 IEEE/RSJ International Conference on*, pp. 2242–2249, IEEE, 2012.

[14] R. Marchant and F. Ramos, "Bayesian optimisation for informative continuous path planning," in *Robotics and Automation (ICRA), 2014 IEEE International Conference on*, pp. 6136–6143, IEEE, 2014.

[15] P. Brass, I. Vigan, and N. Xu, "Shortest path planning for a tethered robot," *Computational Geometry*, vol. 48, no. 9, pp. 732–742, 2015.

[16] S. Kim and M. Likhachev, "Path planning for a tethered robot using multi-heuristic a* with topology-based heuristics," in *Intelligent Robots and Systems (IROS), 2015 IEEE/RSJ International Conference on*, pp. 4656–4663, IEEE, 2015.

[17] S. A. Zanlongo, L. Bobadilla, and Y. T. Tan, "Path-planning of miniature rovers for inspection of the hanford high-level waste double shell tanks," *Florida Conference on Recent Advances in Robotics (FCRAR)*, 2017.

[18] T. J. Barnes and J. R. Gunter, *241-AY-101 Tank Construction Extent of Condition Review for Tank Integrity*. 2013.

[19] C. E. Rasmussen and C. K. Williams, "Gaussian processes for machine learning. 2006," *The MIT Press, Cambridge, MA, USA*, vol. 38, pp. 715–719, 2006.

[20] M. L. Stein, *Interpolation of spatial data: some theory for kriging*. Springer Science & Business Media, 2012.

[21] R. H. Byrd, P. Lu, J. Nocedal, and C. Zhu, "A limited memory algorithm for bound constrained optimization," *SIAM Journal on Scientific Computing*, vol. 16, no. 5, pp. 1190–1208, 1995.

[22] "Radioactive liquid waste facilities," *Savannah River Remediation*, 2017.

[23] S. M. LaValle, *Planning algorithms*. Cambridge university press, 2006.

[24] N. Srinivas, A. Krause, S. M. Kakade, and M. W. Seeger, "Information-theoretic regret bounds for gaussian process optimization in the bandit setting," *IEEE Transactions on Information Theory*, vol. 58, no. 5, pp. 3250–3265, 2012.

[25] J. Snoek, H. Larochelle, and R. P. Adams, "Practical bayesian optimization of machine learning algorithms," in *Advances in neural information processing systems*, pp. 2951–2959, 2012.

[26] E. Brochu, V. M. Cora, and N. de Freitas, "A tutorial on bayesian optimization of expensive cost functions, with application to active user modeling and hierarchical reinforcement learning," *CoRR*, vol. abs/1012.2599, 2010.

[27] M. DiBono, A. Abrahao, D. McDaniel, and Y. T. Tan, "Development and testing of robotic inspection tools for the hanford high-level waste double shell tanks," in *WM Symposia*, 2017.

[28] M. DiBono, D. McDaniel, A. Abrahao, L. Lagos, and Y. T. Tan, "Engineering scale testing of robotic inspection tools for double shell tanks at hanford," in *WM Symposia*, 2018.